Assessment of Supercapacitor performance in a hybrid energy storage system with an EMS based on the discrete wavelet transform

Miguel Robayo[1*], Markus Mueller[1], Suleiman Sharkh[2] and Mohammad Abusara[1]

[1] College of Engineering, Mathematics and Physical Sciences, University of Exeter, UK
[2] Faculty of Engineering and the Environment, University of Southampton, UK
*mr597@exeter.ac.uk

Abstract—
When battery and supercapacitor (SC) Energy Storage Systems (ESSs) coexist in electric vehicles, energy management is imperative to ensure efficient power distribution based on the strengths and weaknesses of each ESS. The decoupling of highly dynamic power demands into components that match the dynamic nature of each ESS is essential. The Discrete Wavelet Transform (DWT) has been widely recommended for this purpose as part of real time energy management systems. However, due to DWT signal processing, delays in the frequency components can undermine the benefits of hybridization. This paper analyses the contribution of the SC to alleviate the battery when the DWT is used with and without time delay compensation using future demand prediction. Four different implementation strategies for a DWT based EMS have been evaluated using different metrics to quantify energy circulation and SC assistance during acceleration and braking. Simulation results using urban and highway driving cycles, show that obtaining the SC current reference as the difference between the real time current demand and the DWT low frequency component enhances SC assistance during acceleration and braking at the expense of higher energy circulation. The complexity added by future demand prediction does not reap SC performance benefits.

***Index Terms*— Hybrid energy storage, Discrete wavelet transform, Electric vehicle, Energy management system, Long-short term memory neural network.**

I. INTRODUCTION

The peak performance of an Electric Vehicle (EV) is determined by the power density of the Energy Storage System (ESS). The ESS must be able to provide/accept high currents that are within its maximum specified discharge rate (C-rate) during heavy acceleration and braking. Additionally, vehicle autonomy is defined by the ESS's energy density. An ESS with high energy and high power densities is necessary for this application. The high energy density and long cycle life of lithium-ion batteries make them the preferred technology for EVs. However, a trade-off between energy and power is inevitable when manufacturing battery cells. Those designed for high-energy applications have a relatively low power capability, which limits their ability to discharge at high current rates and accept high currents during charging. In contrast, battery cells designed for power applications can discharge and accept high currents, but at the expense of energy density. No battery today meets all the requirements of an advanced high performance energy storage for EV application [1].

EV battery packs consist of a serial-parallel arrangement of high energy battery cells that determine the system voltage, energy, and power. To account for the battery cycle life, energy, and the required power density, battery oversizing is a common practice [2]-[4]. However, this causes an increase in the system's weight, volume, and cost. Hybridization of energy storage systems has been widely proposed in the literature as an alternative to battery oversizing [5]-[8]. EV's can be equipped with a Hybrid Energy Storage System (HESS) that combines a high energy density battery pack and a high power density source. Ideally, the high power source should assist the battery to cope with sudden power demands caused by changes in acceleration and recover all the power generated when braking. An improvement in battery life is possible if its load profile is relieved from positive and negative peak power [5]. High energy density batteries with low power capability can be complemented with a high power density source such as a SC, lithium-ion capacitor (LIC) or ultra-high power battery (UHPB), which can deliver rapid bursts of power during high power demand and capture power during braking. SCs are able to discharge and recharge at high rates without compromising their performance over time, however, they suffer from considerable self-discharge. Conversely, UHPB are able to discharge at high rates but their charging rate is significantly inferior compared with SCs. Moreover, lifetime is still affected by temperature build up, which limits its continuous operation at high rates. In this work, SCs are considered due to their capability to charge and discharge at high rates without compromising their lifetime. Nevertheless, the solution developed in this work still apply to high power batteries, however, in this case the EMS must implement additional charge/discharge rate limits to safeguard the lifetime of the power battery. Practical implementation of HESS in electric minibuses have

demonstrated the performance of lithium batteries and SCs to cope with frequent and fast charging cycles and deliver the required power and energy [43].

To control power flow in a HESS, an EMS that operates in real time is fundamental. Different approaches were proposed to achieve this objective, which can be broadly classified into optimization and rule based control strategies [9]. Rule-based EMSs are convenient for implementation in real time controllers due to their simplicity and convenience. These methods are based on empiric human expertise where a set of rules are generally implemented as lookup tables or if-then expressions. Rule-based strategies are classified into deterministic approaches, filtration strategies, fuzzy logic, model predictive control, and neural network based control. With filtration based approaches, power demand can be decomposed into frequency components that match each ESS dynamics. In fully active topologies, the battery and SC power flows are controlled by allocating the low frequency component (LFC) to the battery and the high frequency component (HFC) to the SC. In this work, a semi-active control topology is adopted where the SC power flow is controlled through a bidirectional DC/DC converter, providing the HFC while the battery provides the power difference. Details on semi-active and active topologies can be found in [10]. EMS strategies based on conventional filters, i.e. low (LPF) and high pass filters (HPF), and the Discrete Wavelet Transform (DWT) have been proposed to extract frequency components from the power demand. With conventional filters, phase shift and group delay can cause the filtered signals to exhibit time lags, whereas with the DWT, signal processing introduces long time delays. Using the delayed HFC to control the SC in a semi-active configuration, which is the method preferred by most researchers investigating this topic, results in excess energy being circulated between the battery and SC via the DC-bus. Excess energy is passed through the non-ideal DC/DC converter, which increases the system's energy loss. Besides, the battery does not receive adequate assistance during peak demand due to the delayed response of the SC with respect to real time demand. These issues undermine the SC's primary purpose and the rationale for hybridization. In the literature, the effects of these issues on power distribution, SC assistance and the system's energy efficiency have not been adequately discussed.

Reported literature suggests that the frequency components obtained with the DWT can be used directly to control the battery and SC power contribution despite the delay. Some researchers developed EMS strategies based on 3 levels of decomposition [11]-[19], while others proposed 5 levels [20], [21]. With this approach, the delay caused by the DWT is fixed. Other researchers proposed adaptive methods to control the battery and SC charge/discharge rate by varying the decomposition level of the DWT during runtime [22]-[24]. In this case, however, the delay is variable. Wang et al. [21] performed an evaluation of the performance of an EMS based on the DWT to determine the level of decomposition. This work concluded that for a signal sampled at a rate of 1 Hz, 3 levels of decomposition showed better performance than other decomposition levels. In [25], the level of decomposition was selected by considering the frequency response range of the power sources. For a battery-ultracapacitor system, it was concluded that 2 levels were appropriate while for a fuel cell-ultracapacitor system, 8 levels were recommended. According to our previous analysis [26], a delay of 8s would be introduced in the frequency components with 3 levels of decomposition. Similarly, a delay of 4s is associated with 2 levels of decomposition and 256s with 8 levels, considering the parameters presented in [25] and a sampling rate of 1Hz. Obviously, using the frequency component with such a long delay will generate significant performance deterioration when applied in real time. With the variation of the DWT level of decomposition in adaptive methodologies [22]-[24], the problem with varying delay becomes more challenging. Signal processing with the DWT introduces a considerable delay in the frequency components, which precludes their direct use in real-time applications.

Zhang and Deng [22], presented an adaptive multi-level Haar wavelet transform for allocating power to batteries and SCs. The level of decomposition was variable and determined according to the driving cycle which was identified using a learning vector quantization neural network. It was concluded that a 4th level of decomposition is needed for highway driving cycle, a 3rd level for moderate urban cycle and a 2nd level for congested urban cycle. However, the authors ignored the DWT delay and did not consider its implications in real time, especially when switching between levels of decomposition. In this particular case, the EMS would be required to switch between frequency components depending on the changes in the driving cycle, specifically 4 seconds delay (2 levels of decomposition), 8 seconds delay (3 levels of decomposition) and 16 seconds delay (4 levels of decomposition). Peng et al. [39] proposed a methodology for adaptively varying the DWT level of decomposition between 1 and 5 based on the SOC of the SC. A similar approach was proposed in [23], however this time the level of decomposition varied between 2 and 5. In [40] an adaptive wavelet transform-fuzzy logic control energy management strategy based on driving pattern recognition was proposed. The algorithm used cluster analysis to classify driving cycles into different patterns according to the features extracted from historical driving data in real-time. After recognition results were obtained, an adaptive wavelet transform was employed to allocate the high frequency components of power demand to the SC, while the low frequency component was distributed to battery. Fuzzy logic was used to maintain the SOC of the SC within a desired range. The level of decomposition was varied between 2 and 5 according to a driving pattern recognition algorithm. All the proposed methodologies

presented above have been suggested for real time operation, however, the presence of significant delay in the frequency components was neglected.

Wavelets with high filter order have also been proposed instead of the Haar wavelet to obtain frequency components to control power flow in a HESS. Shen et al. [41], proposed an EMS based on a Symlet wavelet with 3 levels of decomposition and performed an experimental test to validate the strategy. However, important information regarding the order of the Symlet wavelet (between 2 and 20), and the sampling rate were not provided, which made this work difficult to replicate. To depict the delay problem when a high order wavelet is used, suppose that the chosen wavelet was symlet2, which has 4 filter coefficients, and the sampling rate was 1 Hz. The total delay that would be present in the frequency components after 3 levels of decomposition would be 22 seconds with respect to the real time power demand (see eq. 3 and 4). Conversely, the Haar wavelet under the same conditions yields a delay of 8 seconds. Song et al. [42] proposed a wavelet-transform-based energy management strategy using Daubechies 4 (db4) wavelet and 5 levels of decomposition. In this case, the delay introduced by the DWT, considering that the db4 wavelet has 8 filter coefficients, is 218 samples. The sampling rate was not provided, but it is most likely to be between 1 Hz and 16 Hz as it would yield a frequency sub-band between 0-16 mHz and 0-250 mHz, which is the range required for this application, with corresponding time delays between 218 seconds and 13.6 seconds, respectively. Higher sampling frequencies would yield high frequency components with very small energy content, which would result in the SC providing little to no assistance to the battery. Obviously, higher order wavelets results in longer time delays. Although the shortest time delay can be achieved with the Haar wavelet, dealing with the delay in real time applications remains a challenge.

Other studies have suggested that power demand prediction can be used to compensate for the DWT delay to enable real time operation, however, they failed to demonstrate the benefits/drawbacks of prediction in terms of SC performance. A delay compensation approach was presented in [27], where a nonlinear autoregressive neural network was trained to perform power demand predictions to compensate for the DWT delay (3.2s) when the power demand, sampled at 10 Hz, was decomposed into 5 levels. The predicted HFC was used to control the SC. The neural network consisted of one hidden layer with 10 neurons, which was trained to predict 32 future samples based on the previous 60 samples. The training dataset consisted of a power demand time series that resulted from a low speed (24 km/h peak) driving cycle with a smooth pattern that was repeated 2 times over a long-time span (13000s). The trained network was, unfortunately, exposed to the same driving pattern during testing. In addition, driving cycles representing real-world driving schedules, where power demand is highly variable, were not used to test the generalization ability of the trained network. Furthermore, this study did not compare SC performance before and after time delay compensation, making it impossible to determine whether the prediction strategy improved the system's performance. Zhang et al. [28], proposed a real time EMS for battery-SC HESS based on a combination of DWT, neural network, and fuzzy logic. A 2-level DWT was used to decompose the power demand signal associated with 9 standard driving cycles. The obtained DWT LFC along with the load power demand were used as inputs to train the neural network with the aim to predict the low frequency power demand. However, the chosen prediction window was not in agreement with the delay generated by the DWT.

There is a scarcity of research detailing the implementation of the DWT as part of a real time EV EMS in light of delay issues. Most of previous studies suggested the direct use of the DWT HFC to control the SC [11]- [19] as evidenced in Table I, but there is little work done to compare this with other possible implementations such as obtaining the SC current as the difference between total current and DWT LFC with and without prediction. Furthermore, the analysis of whether delay compensation improves the SC performance in terms of timely assistance during motoring and braking and its influence on energy efficiency has not been addressed. The energy efficiency problem arises from the fact that in addition to the total amount of energy supplied/recuperated by the HESS to match the load requirements during a given driving cycle, additional energy is circulated between the battery and the SC through a non-ideal DC/DC converter which results in additional power loss.

Many researchers who applied the DWT method for filtration purposes have, unfortunately, overlooked the effect of delay in the practical implementation. Moreover, the sampling frequency was not even indicated in some published papers, e.g. [11]-[14], [17]-[20], [24], making it difficult to calculate the delay and the frequency sub-band allocated to the SC. Time delay compensation strategies were suggested in [15], [16], and [27]. However, no evidence was provided that this has indeed improved the performance or efficiency of the system. This work specifies the mechanism used to calculate the delay, assesses the effects of the delay on the HESS power distribution, and evaluates the SC's effective contribution during motoring and braking with and without time delay compensation. There has never been an analysis of this type before, and that makes this work unique.

Table I, summarises the issues mentioned before as they were encountered in published work.

TABLE I. LIST OF ISSUES FOUND IN PREVIOUS WORK

Reference	Time delay addressed?	EMS strategy	Comments
[22], [23], [39]	No	DWT high frequency allocated to the SC	Adaptive method to switch between levels of decomposition. Variable delay not considered. Sampling frequency not given by [22], 100 Hz for [23] and 1 Hz for [24]. Frequency sub-bands not specified.
[11], [12], [13], [14], [17], [18], [19], [20], [24], [28], [40], [41], [42]	No	DWT high frequency allocated to the SC	Fixed level of decomposition. Sampling frequency not given. Frequency sub-band not calculated
[15], [16], [27]	Yes	Predicted DWT high frequency allocated to the SC	Fixed level of decomposition. Comparison of performance before and after prediction not included [27] tested the trained network with the same dataset used for training

Considering the background presented, an analysis of the effective contribution of the SC to alleviate the battery during motoring and braking with respect to real-time implementation of the DWT is missing in the literature. Therefore, this paper analyses and compares 4 EMS strategies based on the DWT that are different in the way the SC current reference is determined. Firstly, the DWT HFC is used directly to control the SC. Secondly, a LSTM neural network is trained to perform power demand predictions to compensate for the DWT delay and then the predicted DWT HFC is used directly to control the SC. Thirdly, the HFC is calculated as the difference between the real time current demand and the DWT LFC. Finally, the third approach is replicated with the predicted DWT LFC. The performance of the mentioned strategies are thoroughly assessed and compared using 4 metrics as follows:

1. SC effective motoring assistance: amount of energy supplied by the SC during positive demand.
2. SC assistance during positive current rate (peak assistance): SC assistance during acceleration (periods of positive current demand rate of change)
3. SC braking energy recovery: amount of energy recuperated by the SC (braking assistance).
4. Energy circulation: energy circulated between the battery and SC.

A detailed Matlab-Simulink model of an EV is developed to test the EMS strategies with a variety of driving cycles representing real-world loading conditions including urban and highway scenarios. The contributions of this paper are summarized as follows:

a) Investigation of energy circulation between the battery and SC as a consequence of the DWT time delay.
b) Investigation of different real time implementation of EMSs based on the DWT, considering energy circulation and SC assistance during motoring, acceleration, and braking.
c) Design of a LSTM neural network to predict future power demand before it is fed to the DWT to compensate for the time delay. Unlike neural networks presented in the literature, this network has been trained offline using power demand corresponding to 8 different standard driving cycles and tested using 4 driving cycles not included in the training dataset to ensure network generalization capability.
d) Evaluation of the effectiveness of time delay compensation in improving the SC performance in a HESS controlled with an EMS based on the DWT.

II. SYSTEM MODELING

A. Vehicle and power train Characteristics

The schematic of the EV model used in this study is shown in Fig. 1.

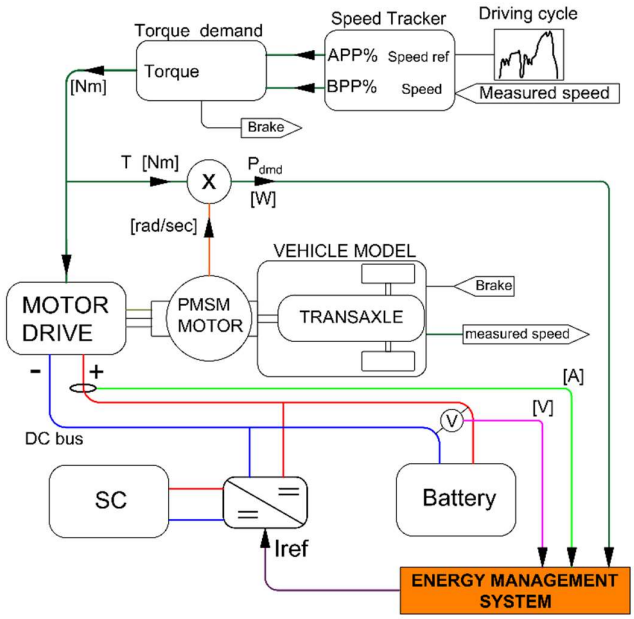

Fig.1. System Schematic

The vehicle and power train characteristics are presented in Table II. The tractive force required to move the vehicle can be calculated as explained in [29]. The electric motor must overcome gravitational f_g, aerodynamic f_{Aer}, inertial f_{acc}, and rolling resistance f_{roll} forces acting against the movement of the vehicle. Thus, the tractive force f_{Tr} required to move the vehicle can be expressed as:

$$f_{Tr} = f_g + f_{Aer} + f_{acc} + f_{roll} \tag{1}$$

$$f_{Tr} = M_{vh} g \sin\alpha + \frac{1}{2}\rho C_d A_{vh} V_{vh}^{\ 2} + M_{vh}\dot{V}_{vh} + M_{vh} g \cos\alpha C_{rr} \tag{2}$$

where M_{vh} is the mass of the vehicle, g is the gravitational acceleration, α is the road gradient angle, ρ is the air density assumed to be that of dry air at 20°C, C_d is the aerodynamic drag coefficient, A_{vh} is the vehicle's frontal area, V_{vh} is the velocity of the vehicle, $\dot{V}_{vh}$ is the vehicle acceleration and C_{rr} is the rolling resistance coefficient. The road gradient angle is assumed to be zero.

The braking strategy is based on a fixed ratio between electric and mechanical braking forces as presented in [30]. The braking model consists of a parallel braking strategy, where the regenerative torque of the motor is exerted on the front driving axle directly in addition to the friction brake. In passenger cars with a single motor, regenerative braking is better utilized when the electric motor is installed on the front axle [30]. The mechanical brake has a fixed ratio distribution of 80% on the front and 20% on the rear brakes. The electric motor brake is controlled by the vehicle controller based on vehicle speed, brake pedal position, and the State of Charge (SOC) of the SC. When the wheel speed is lower than 15 km/hr, due to either very low vehicle speed or wheel speed close to lock up, the electric brake produces no braking force and braking is produced only by the mechanical system. When the speed is higher than a set threshold and the SC is able to accept charge, the following braking actions are performed considering the deceleration rate:

a) When the vehicle deceleration is less than 0.15g (g = 9.81m/s^2), all the braking force is produced by electric regenerative braking and no mechanical force is applied to the front and rear wheels, emulating the internal combustion engine retarding function.
b) When the vehicle deceleration is between 0.15g and 0.7g, 80% of the total braking force is allocated to the front axle and 20% to the rear axle. The electric and friction brakes work together to meet the required braking force on the front axle. The rear axle brake is purely mechanical. The maximum electric force is generated when the deceleration is close to 0.15g and minimum when it is close to 0.7g. The reduction in the electric braking force is linear.
c) Any deceleration above 0.7g is considered emergency braking and therefore braking is performed by the mechanical system only.

TABLE II
VEHICLE AND POWERTRAIN CHARACTERISTICS

Vehicle Characteristics		
Mass (kerb weight)	1662	kg
Aerodynamic drag	0.28	
Rolling resistance coefficient	0.012	
Front area	2.27	m^2
Air density	1.204	kg/m^3
Powertrain characteristics		
Maximum Torque	340	Nm
Maximum Power	160	kW

B. Hybrid Energy Storage System

a. Battery Model

The battery model is based on the work presented in [31], which constitutes the basis for the generic battery model readily available in Matlab-Simulink. This model represents accurately the battery voltage dynamics in the presence of variable charging and discharging currents by considering the open circuit voltage as function of SOC. The parameters for this model can be easily extracted from the battery manufacturer's discharge curve in steady state. The battery parameters used in this paper are summarized in Table III.

TABLE III
BATTERY CHARACTERISTICS

NCR21700A, 5000mAh		
Cell specific energy	264.2	Wh/kg
Cell weight	70	g
Pack nominal voltage	350	V
Pack maximum Capacity	120	Ah
Fully Charged voltage	407	V
Cut-off voltage	262.5	V
Pack configuration	96 series, 24 parallel	
Pack energy	42	kWh
Pack internal resistance	48	mΩ
Pack specific Energy	163	Wh/kg
Cont./pulse discharge C-rate (2C/3C)	240/360	A
Charge C-rate max (0.6C)	72	A

b. Supercapacitor Model

The SC is based on the Stern-Tafel model which reproduces the double layer capacitance related to the nonlinear diffusion dynamics by a combination of the Helmholtz's capacitance and the Gouy-Chapman's capacitance [32]. This model is the basis of the generic SC block available in Matlab-Simulink. Default Simulink parameters for the Stern equation are selected along with the characteristics shown in Table IV.

TABLE IV
SUPERCAPACITOR CHARACTERISTICS

Maxwell BCAP 3400		
Cell capacity	3400	F
Cell Equivalent DC series resistance	0.15	mΩ
Cell Rated voltage	3	V
Cell specific power	14.5	kW/kg
Cell weight	496	g
Pack configuration	135 series, 1 parallel	
Pack Voltage (max)	405	V
Pack capacity	25.2	F
Pack resistance	20	mΩ
Pack Specific Energy	5.36	Wh/kg

The optimal sizing of the HESS is not within the scope of this work. However, the battery capacity is similar to that of the Nissan Leaf battery (40 kWh), while the SC pack was sized using a single string of 3400F SCs with a total voltage of 405V. Of course, different combinations of battery and SCs can be designed, however, weight, volume, and cost need careful consideration.

III. ENERGY MANAGEMENT SYSTEM

A. The Discrete Wavelet Transform

The DWT is a technique that allows the translation of a time domain signal into a signal localized in both the time and frequency domains with pre-specified detail resolutions. The multi-resolution decomposition obtained with the DWT offers a very powerful method for the analysis of signals that feature HFCs short durations and LFCs

for long durations [33]. HFCs are obtained from the DWT detail coefficients whilst the LFC is obtained from the DWT approximation coefficient. The decomposition process results in one DWT approximation coefficient (lowest frequency sub-band) and a number of DWT detail coefficients that depend on the sampling frequency and chosen level of decomposition. The sampled version of the original signal can be perfectly reconstructed from the DWT coefficients by means of the inverse DWT. Specific frequency sub-bands can be isolated and reconstructed with this procedure. However, the reconstructed DWT frequency components carry a delay that is influenced by the sampling frequency, the target low frequency sub-band (approximation component), and the chosen wavelet function. This delay makes the direct use of the DWT frequency components troublesome in real time controllers. The delay results from adding the current sample time period (T_s) to the product between T_s and number of previous samples N_s required to perform a given level of decomposition. The delay (T_d) is given by:

$$T_d = T_s(1 + N_s) \tag{3}$$

where N_s can be calculated according to [34] such as:

$$N_S = \sum_{i=1}^{j}(N_f - 1)2^{i-1} \tag{4}$$

N_f is the order of the filter, characterized by the number of coefficients associated with the chosen orthogonal wavelet base, i is the current level of decomposition and j is the final level of decomposition. The number of samples grow exponentially with the increase of levels of decomposition. The delay is exacerbated as the order of the filter increases when using different wavelet bases other than the Haar wavelet. Haar is the simplest wavelet with the smallest filter order ($N_f = 2$).

B. DWT in EMS, Energy Circulation and SC Assistance

To illustrate energy circulation between the battery and SC in a semi-active topology, the SC current reference is first obtained with a conventional first order HPF. This will enable the observation of the exacerbated energy circulation when the SC current reference is obtained later with the DWT. At certain frequency range, the output of the HPF has a response that is proportional to the time derivative of the input. Thus, when the slope of the current demand signal (measured at the DC-bus) changes from positive to negative, the output of the HPF will also change from positive to negative. For example, when the driving cycle demands a reduction in acceleration i.e. from acceleration to cruising, the current demand declines but remains positive. However, this drop in current demand can appear as a negative signal at the output of the filter even though there is no braking command requested. Fig. 2 illustrates this event with a conventional first order HPF with a cut-off frequency of 125 mHz. The current demand and the vehicle speed from t=20s to t=37s of the Federal Test Procedure 72 (FTP72) driving cycle are displayed. At time t = 26s the slope of the current demand changes from positive to negative because of the drop in the power demand caused by an adjustment in speed. Although speed keeps rising from 26 km/h at t = 26s to 28 km/h at t = 27.6s (i.e. no braking command), the HPF output becomes negative. As the SC is controlled with the output of the HPF, energy circulation occurs as the SC is commanded to recharge (negative current command represented as green shades) even when no braking power is generated. The SC is recharged from the battery (orange shades), which transfers power to the SC through the DC/DC converter. The areas shaded in light blue represent the effective contribution of the SC during motoring and braking.

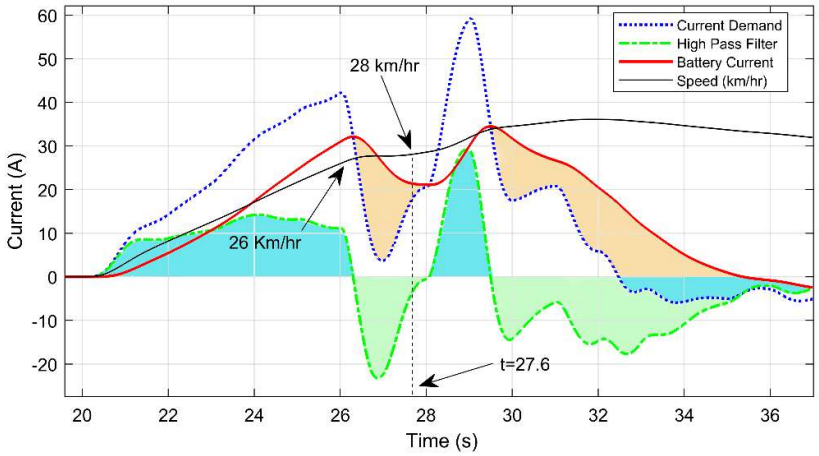

Fig.2. 1st order HPF. Energy circulation

Energy circulation is exacerbated when the DWT is used, as the HFC is delayed with respect to the real time demand. In Fig. 3a, the SC follows the HFC current reference obtained with the DWT. The current demand is sampled at 1 Hz and then decomposed into 2 levels to obtain a frequency sub-band of 125-500 mHz. The drop in the current demand that starts at t = 26s results in a delayed drop in the DWT HFC that starts at t = 30s (delay = 4s). Thus, the use of the DWT HFC results in the SC recharging when there is no braking power (green shaded areas), forcing the battery to provide power to keep the system's balance (orange shaded areas). Consequently, more stress is imposed on the battery rather than alleviating it, and poor SC contribution is observed during motoring and braking (light blue shaded areas). Moreover, efficiency decreases as energy needs to be circulated via a non-ideal DC/DC converter.

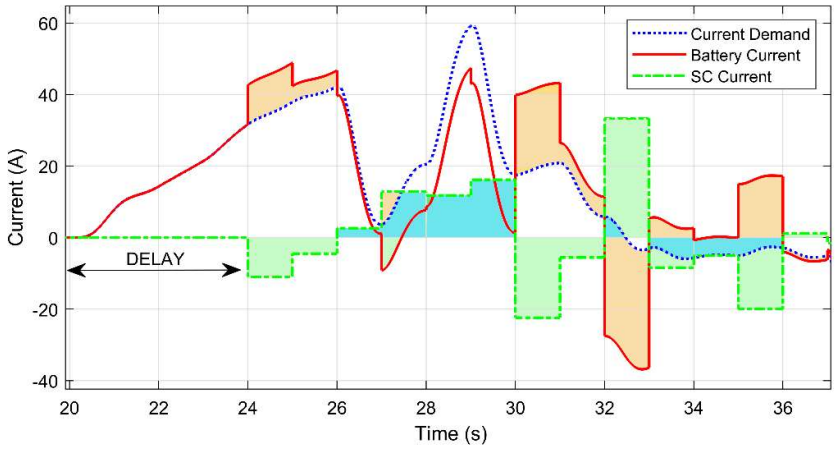

Fig.3a**.** DWT HFC as SC current, sampling=1Hz,

DWT HFCs with more details (smoother signal) can be generated with higher sampling rates and adequate levels of decomposition. In Fig.3b, sampling rate of 32 Hz and 7 levels of decomposition result in frequency sub-band of 0.125Hz-16 Hz. The delay remains unchanged (4s).

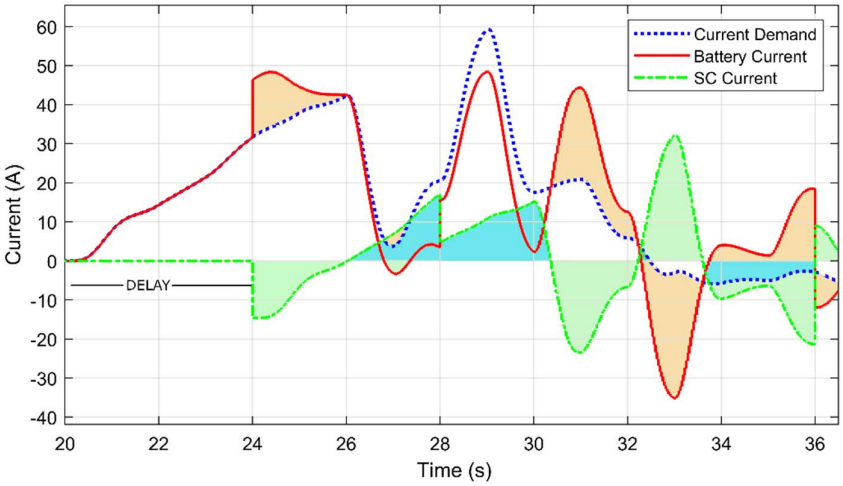

Fig.3b. DWT HFC as SC current, sampling =32 Hz.

Both Fig.3a and 3b show that the SC is not assisting the battery during acceleration and is partially recovering power generated during braking. This is evident between t=20 and t=26, and between t=33 and t=36, respectively.

To quantify the effectiveness of the SC assistance during motoring and braking, a comparison with a benchmark reference is necessary. To determine this reference, the following factors have been considered:

1. The first derivative of the positive current demand is calculated to define time windows that correspond to positive current demand changes. Only positive values are considered. Time windows are shown in Fig. 4 for t=19s to t=42s of the FTP72 driving cycle.

2. During positive current rate, the benchmark current reference is set to match the first derivative of the current as long as the derivative is less than the total current demand, otherwise it is set to match the total current demand. This makes the benchmark reference proportional to the rate of change of current but without exceeding the total current demand. This defines the areas where SC assistance would be most beneficial.
3. During braking, all the generated energy should be absorbed by the SC if its SOC allows it. Otherwise, it will be allocated to the battery observing the maximum charging C-rate. This area is given by the negative current demand.

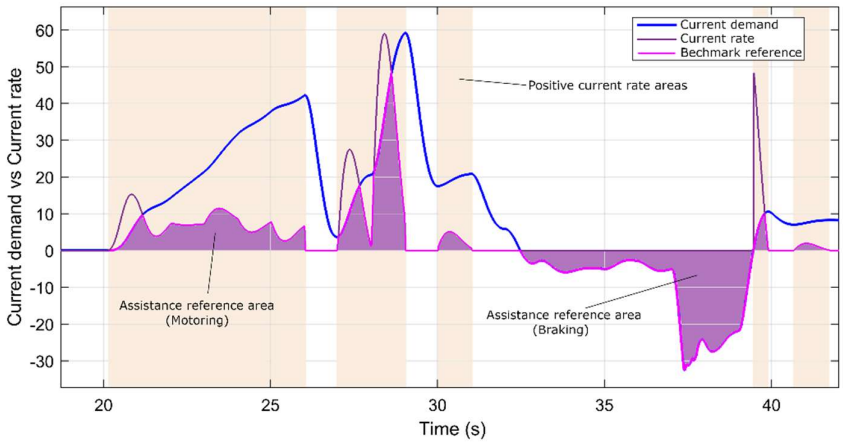

Fig. 4. Reference signal to assess SC performance

The effectiveness of SC assistance with different EMS approaches can be assessed by comparing the energy provided by the SC against the energy of the benchmark reference area. The energy E in Wh is calculated as follows:

$$E = \frac{1}{3600}\int_0^t I_X \times V_{DC-link}\,dt \tag{5}$$

where I_X is the current of the variable being analysed i.e. total, battery, and SC currents. $V_{DC-link}$ is the voltage of the DC-link. Positive current demand is used to calculate motoring energy and negative current demand to calculate braking energy. For each EMS strategy presented in this paper, the areas shown in Fig. 5 are calculated. The orange shading represents the circulation energy (unit is Ah) supplied by the battery and received by the SC (green shading), or viceversa. The blue shaded areas represent the SC effective contribution during the motoring and braking stage. The purple area represents the current reference based on the current rate of change. These areas are used to quantify the SC assistance during motoring, acceleration, braking and total energy circulation for different EMS strategies.

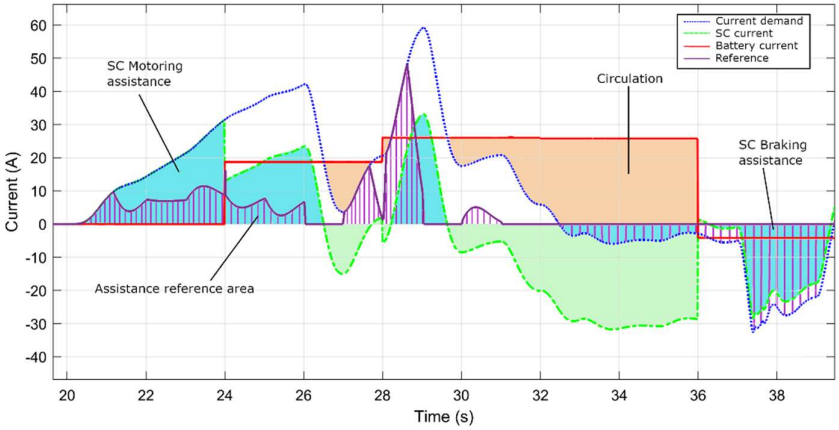

Fig. 5. Calculated areas to compare the performance of the SC with different EMS strategies

C. *Long-Short Term Memory Neural Network*

Power demand prediction has been proposed in the literature as a way to mitigate delay and enable the DWT to work in real time. LSTM neural networks are a type of Recurrent Neural Networks (RNNs) that perform well when learning long term temporal dependencies. RNNs carry out prediction of future steps by considering previous data. The internal structure of the network learns from earlier stages and uses this previous data along with new data to forecast future steps. However, typical generic RNNs can remember only a few previous steps in the sequence and therefore fail to remember long sequences of data [35]. On the other hand, long term memory is possible by using LSTM networks, which are designed to capture and store data. The LSTM cell behaves like a memory with the ability to write, read and delete data according to the decisions stipulated by its input, output, and forget gates. Details about the functions and characteristic equations of each gate can be found in [36]-[37]. In this work, the hyper-parameters of the LSTM network were determined by testing several architectures and comparing their prediction Mean Squared Error (MSE) as shown in Table V. A good fit learning curve is identified when the training and validation loss decrease to a point of stability with a minimal gap between the two final loss values [38].

TABLE V
LSTM NETWORK ARCHITECTURES

LSTM Structure	Layers and Neurons	Epochs	Training Loss MSE (kW)	Validation Loss MSE (kW)
1	1x10	10	59.16	29.65
2	1x10	50	51.71	32.64
3	2x10	50	55.44	28.18
4	1x50	100	37.57	30.03
5	2x50	100	22.01	41.62
6	2x50	150	13.89	14.78
7	2x50	170	12.78	12.50
8	3x50	150	20.23	15.16
9	1x60	100	34.61	32.71
10	1x100	100	25.59	34.31
11	1x600	50	19.24	12.46
12	1x800	50	17.29	9.56
13	1x1000	50	21.49	14.50
14	1x1100	50	17.91	11.66
15	1x1500	50	24.34	11.30

LSTM structure 7 from Table V is chosen. The selected hyper-parameters correspond to those where the training and validation losses converged and reached a minimum, 12.78 and 12.50, respectively. This was achieved using the stochastic gradient descend optimization algorithm ADAM, a learning rate of 0.001, and hyperbolic tangent (TANH) activation. The neural network structure consists of a sequence input layer receiving 8 samples, 2 fully connected hidden layers with 50 LSTM units each, and a regression layer with 5 outputs, corresponding to the number of predicted samples. The network was trained with 85% of the dataset and tested with 15%. The model's hyper-parameters were tuned to achieve good performance considering the following conditions:

a) The network must predict from the measured real time raw data, as there is no time to perform data pre-processing such as de-noising, normalization, and standardization, which would introduce more delay.
b) The network must be able to perform the prediction with minimum delay.
c) Prediction error must be minimal for any driving condition.

Forecasting based on raw data has some limitations and drawbacks, such as computationally demanding training phases, the need for a big dataset, a large number of hyper-parameters, and sensitivity to measurement noise. The LSTM neural network was created and trained in Keras, a deep learning Application Programming Interface (API) written in Python, using a dataset (duration=8465s) containing the power demand obtained by simulating the vehicle with a battery only ESS with the following 8 driving cycles:

1. Artemis Urban
2. Urban Dynamometer Driving Schedule (HUDDS)
3. Highway Fuel Economy Test (HWFET)
4. JC08 Japanese Chassis Dynamometer Test
5. Unified Dynamometer Driving Schedule LA92
6. Chassis Dynamometer Test SC03
7. EPA Driving Schedule for Light-Duty Vehicles and Trucks (US06)
8. Worldwide Harmonized Light Vehicle Test Procedure (WLTP3).

The power demand associated with any driving cycle depends on several factors including driving style, road

condition, road gradient, weather, traffic conditions, etc. This makes accurate prediction difficult. Due to the complex non-linearity of the power demand associated with driving, prediction errors are inevitable, especially with multi-step time series forecasting. The generalization capability of the trained network is tested with 4 driving cycles not seen by the network during training, obtaining a prediction Root Mean Squared Error (RMSE) of 8.91 kW for the FTP72, 5.75 kW for the Inspection and Maintenance Driving Schedule (IM240), 3.31 kW for the Extra Urban Driving Cycle (EUDC), and 16.19 kW for the Artemis Motorway, when predicting 5 future samples. Additionally, the prediction RMSE for the US06 driving cycle is 11.79 kW and 3.59 kW for the WLTP3 driving cycle, which were used during the training stage. Predictions were executed in a machine with an 8th generation Intel Core i5, 32 GB RAM, 1.9 GHz processor. On average, the network took 0.9s to execute the predictions. This extra delay is variable and is highly dependent on the performance of the computer used. In our previous work [26], this delay was around 2s when a computer with an older processor and smaller memory was used. This extra delay is added to the DWT delay yielding a total of ~4.9s. Power demand is sampled at 1 Hz, hence the prediction window of 5 samples.

IV. EMS PERFORMANCE EVALUATION

In this section, 4 different real-time implementation strategies for the DWT are evaluated in terms of SC assistance during motoring, peak assistance, braking energy recuperation and energy circulation. The 4 strategies depend on how the SC reference current is determined, i.e. $I_{ref(SC)}$ is given by:

A. DWT HFC
B. Predicted DWT HFC
C. Difference between the real-time current demand and the DWT LFC
D. Difference between the real-time current demand and the predicted DWT LFC

A schematic of these 4 strategies is shown in Fig. 6. The detailed EV model developed in II is implemented in Matlab-Simulink along with the DWT strategies and tested using a variety of driving cycles representing real-world loading conditions including urban and highway scenarios. The battery and SC initial SOC is set to 80% for simulations. The sampling frequency is 1Hz and the DWT level of decomposition is 2, which produces a delay of 4s.

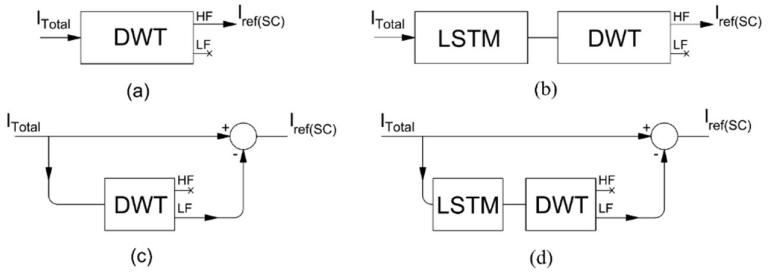

Fig. 6. a) Direct DWT HFC, b) predicted DWT HFC, c) Difference between current demand and DWT LFC, d) Difference between current demand and predicted DWT LFC

A. DWT high frequency component

The current demand associated with the FTP72 driving cycle is sampled at 1Hz and decomposed into 2 levels. The DWT HFC (125mhz -500 mhz) is used directly to control the SC power flow. Because the control signal is delayed, energy is circulated between the battery and the SC, putting greater stress on the battery as it supplies more power to recharge the SC while receiving minimal assistance during the periods of positive changes in current demand. This is evident in Fig. 7, where at t = 57s, the current demand is 41 A, but the battery supplies 68 A as the SC is commanded to recharge. In addition, the SC does not provide assistance during the initial acceleration (t=20s to t=26s) and fails to recuperate braking power, which is mostly absorbed by the battery. SC assistance during motoring and braking is represented by the shaded areas to highlight the effective contribution of the SC.

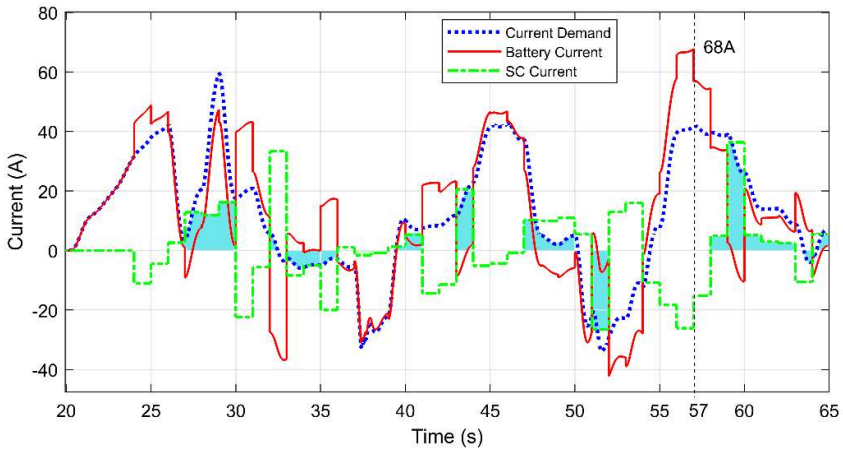

Fig 7. DWT HFC allocated to the SC

The total energy required by the system during motoring is 1668 Wh and the energy produced during braking is 470.8 Wh. This is calculated according to (5) using the current demand. The same procedure is used to calculate the battery and SC energies using the battery and SC current, respectively. The battery provides a total of 1765 Wh during motoring and recovers a total of 569.4 Wh during braking. The SC provides 426 Wh during motoring and recovers 399.4Wh during braking.

Fig. 8 shows the energy balance for the motoring stage. The battery and the SC provided a total of 2191 Wh (1765 Wh+426 Wh) of motoring energy which is equivalent to 31.3% (523 Wh) more energy than the required (1668 Wh) during the driving cycle. From the 426 Wh provided by the SC during the motoring stage, 227.4 Wh are effectively contributed to motoring. A total of 7 Wh is lost due to DC/DC conversion. The remaining 191.6 Wh are transferred to the battery, producing a loss of 5.7 Wh. On the other hand, from the 1765 Wh provided by the battery, 1440.6 Wh are effectively contributing towards motoring while 324.4 Wh are transferred to the SC through the DC/DC converter. This generates a loss of 9.7 Wh. Conversion losses are calculated assuming a DC/DC converter efficiency of 97%.

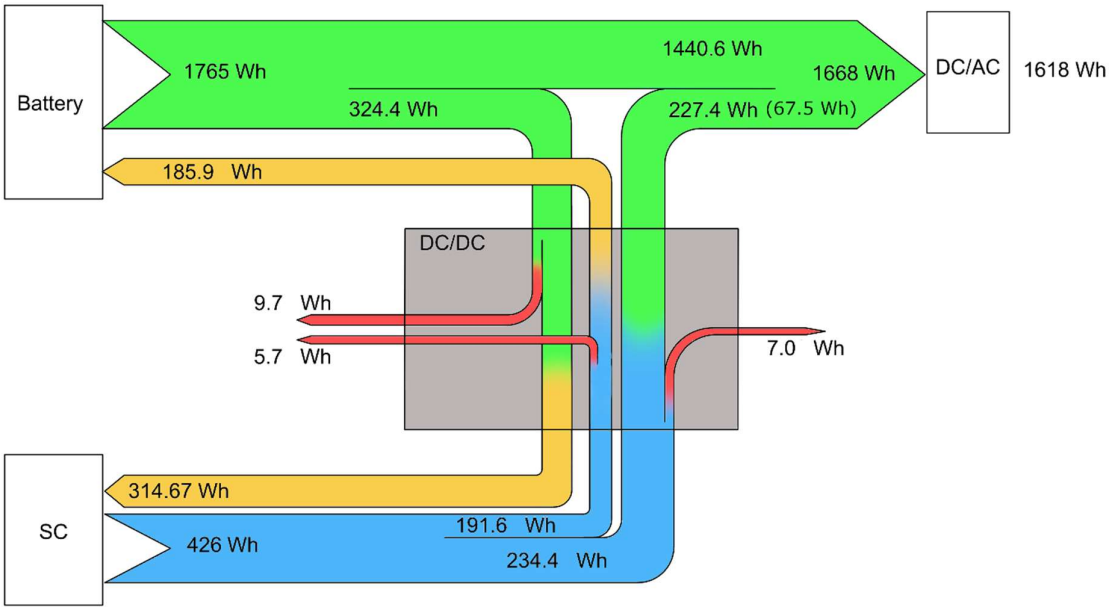

Fig. 8 Motoring stage energy balance

The SC provides a total of 227.4 Wh of effective assistance during the motoring stage, which correspond to the positive blue shaded areas in Fig. 7. However, only 67.5 Wh corresponds to assistance during positive changes in the current rate. This is shown as the positive blue shaded areas in Fig. 9, which depicts a comparison between the SC current and the benchmark reference (see Fig. 4).

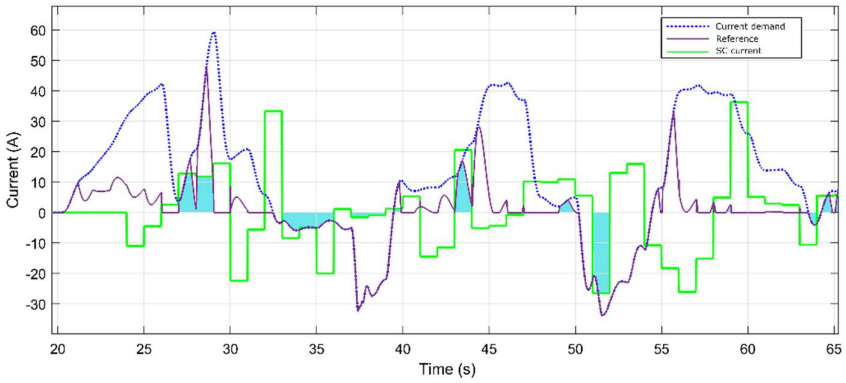

Fig.9. Comparison between the SC current and current rate reference

The energy balance for the braking stage is shown in Fig. 10. The SC recovers only 84,7 Wh of the 470.8 Wh generated during braking (negative areas in Fig.9). The battery absorbs the remaining 383.5 Wh. The same analysis is performed for the other strategies presented in this paper as detailed in the next subsections.

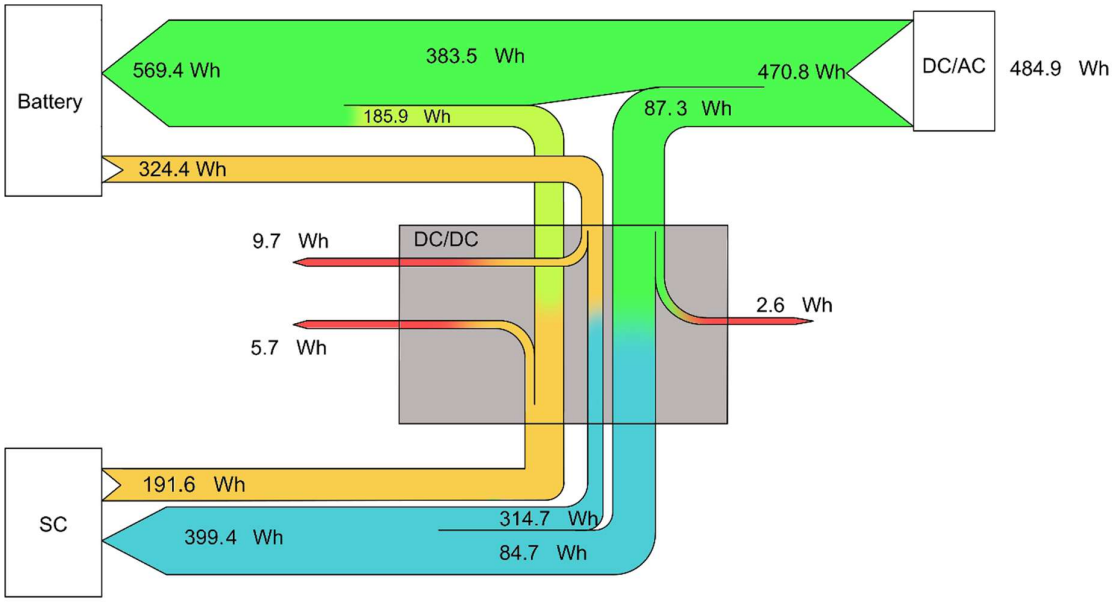

Fig. 10. Braking stage energy balance

B. Predicted DWT High Frequency component

In Fig. 11, the predicted DWT HFC is allocated to the SC according to the strategy presented in Fig. 6b, relieving the battery from excessive energy circulation when compared to approach A (see Fig. 7) as a consequence of delay compensation. However, the battery still lacks SC assistance during acceleration and braking. With the predicted DWT approach, the battery recoups most of the generated braking power. Delay compensation with the prediction approach reduces energy circulation but it is still not sufficient to fulfil the objective of the SC in the HESS as it doesn't assist the battery during acceleration and fails to recover all the braking power. The effective contribution of the SC is represented by the shaded areas.

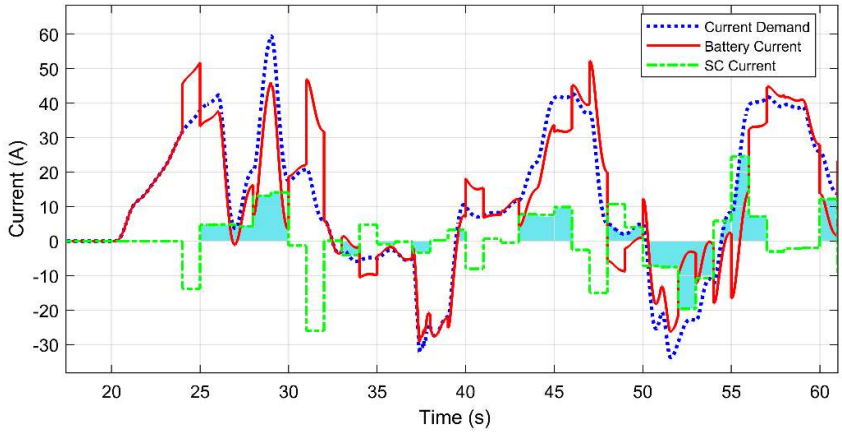

Fig.11. Predicted DWT HFC allocated to the SC

C. High frequency derived as the difference between the real-time current demand and the DWT Low frequency component

Current demand (I_{Total}) is decomposed (2 levels) with the DWT into low and high frequencies. The LFC is subtracted from the current demand (I_{Total}) to obtain the SC current reference according to Fig. 6c. The SC assists the battery during acceleration and peak demand during motoring (positive current demand) and recuperates most of the braking current generated as shown in Fig. 12. However, energy circulation increases between the battery and SC, for example between t=30s to t=36s. With this approach, the SC provides higher energy to assist the battery during motoring and further relieves the battery from braking compared to strategies A and B.

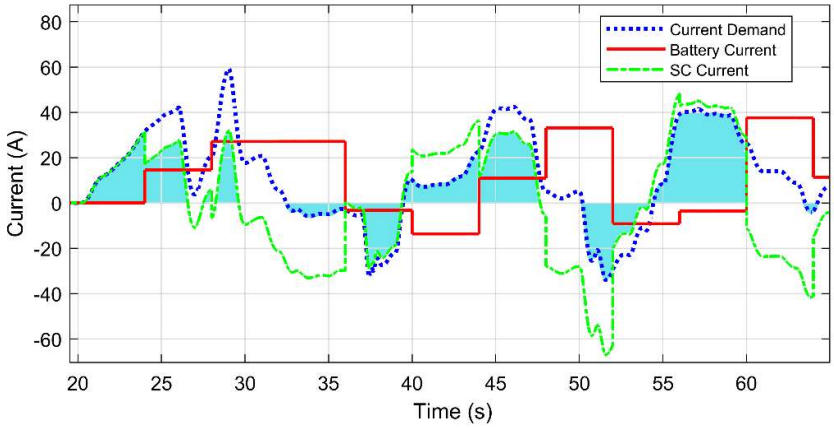

Fig. 12. Current distribution when $I_{ref\,(SC)} = I_{total} - DWT_{LFC}$

D. High frequency derived as the difference between the real-time current demand and the predicted DWT Low frequency component

Using the difference between the current demand and the predicted DWT LFC (Fig. 6d) results in the SC providing assistance during peak demand which is evident between t=20s to t=25s, t=40s to t=45s and from t=54s to t=56s in Fig. 13. Additionally, the SC recovers most of the power generated during braking. Shaded areas depict the SC effective contribution.

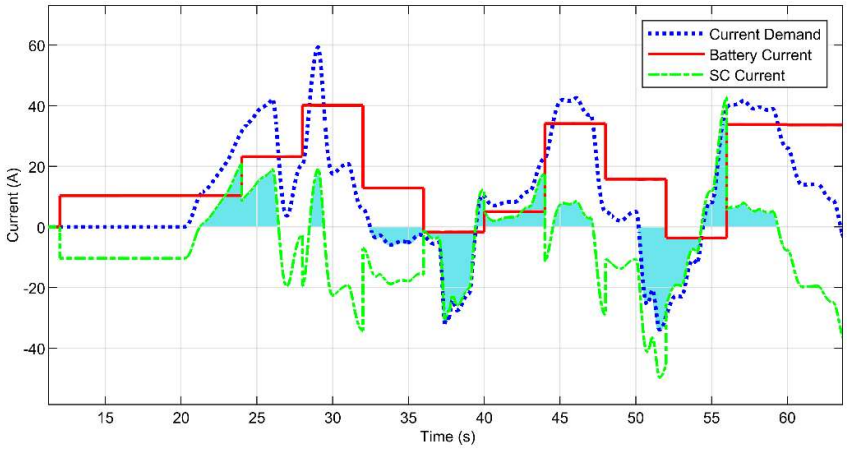

Fig. 13. Current distribution when $I_{ref(SC)} = I_{total} - predicted(DWT_{LFC})$

E. Performance comparison

It is obvious that strategies C and D offer the best results in terms of SC assistance during motoring and braking. However, a meaningful comparison requires an analysis of the effective contribution of the SC, especially the assistance given during positive current rate, and braking. These are referred as SC performance. Table VI shows the results for the EMS strategies presented in this paper with four different driving cycles.

TABLE VI SC PERFORMANCE COMPARISON

Driving cycle	**Strategy (ranking)**	**Energy Circulation (Wh)** (Additional Energy on top of: FTP72=1668 Wh, US06=2601 Wh, WLTP3=3616 Wh Artemis=5525 Wh)	**Effective motoring assistance (Wh)** (FTP72 Max=1668 Wh) (US06 Max=2601 Wh) (WLTP3 Max=3616 Wh) (Artemis=5525 Wh)	**Assistance during positive current rate (Wh)** (FTP72 Max=306.6 Wh) (US06 Max=587.4 Wh) (WLTP3 Max=366.2 Wh) (Artemis=979.6 Wh)	**SC braking recovery (Wh)** (FTP72 Max=470.8 Wh) (US06 Max=452.9 Wh) (WLTP3 Max=755.7 Wh) (Artemis=565 Wh)
FTP72 (Urban)	**A**(3)	31.4%	13.6%	22.0%	18.0%
	B(4)	19.0%	12.8%	18.5%	10.9%
	C(1)	44.0%	34.7%	59.8%	63.4%
	D(2)	33.9%	19.9%	41.1%	22.5%
WLTP3 (Mixed)	**A**(4)	17.4%	8.1%	21.9%	15.0%
	B(3)	16.5%	9.9%	23.3%	13.1%
	C(1)	33.0%	26.0%	76.7%	57.0%
	D(2)	20.6%	17.4%	55.3%	24.5%
US06 (Motorway)	**A**(3)	27.6%	15.7%	17.0%	22.1%
	B(4)	18.5%	9.6%	8.8%	11.4%
	C(2)	34.6%	32.5%	44.0%	57.0%
	D(1)	33.3%	44.3%	73.5%	95.4%
Artemis Motorway	**A**(3)	20.5%	12.2%	20.5%	16.6%
	B(4)	14.2%	9.4%	19.1%	16.7%
	C(2)	24.7%	23.9%	42.0%	70.1%
	D(1)	14.7%	51.2%	70.2%	97.7%

a) Direct DWT HFC (Strategy A) vs Predicted DWT HFC (Strategy B)

The direct use of the DWT HFC to obtain the SC current reference (strategy A) results in low SC effective assistance caused by a delayed response of the SC with respect to the real time demand. The percentage of SC effective motoring assiatance is calculated as the ratio between the SC positive energy contribution to the total positive energy demand (FTP72=13.6%, WLTP3=8.1%, US06=15.7%, Artemis=12.2%). Prediticting the DWT HFC (strategy B) results in a reduction of the SC performance influenced by the prediction error. The SC performance during motoring and braking is reduced for the FTP72, US06 and Artemis driving cycles which have RMSE of 8.91 kW, 11.79 kW and 16.19 kW, respectively. For the FTP72 the SC effective contribution is reduced from 13.6% to 12.8% for the US06 it is reduced from 15.7% to 9.6%, and for the Artemis motorway is reduced from 12.2% to 9.4%, as shown in Table VI. The smaller prediction error obtained for the WLTP3 driving cycle (RMSE=3.59 kW) results in a marginal improvement in the SC effective contribution, as it rises from 8.1% to

9.9%. However, SC performance during braking is reduced from 15% to 13.1%.
With regards to energy circulation, predicting the power demand to compensate for the DWT HFC delay (Strategy B) leads to an expected reduction when compared to direct use of the DWT HFC (Strategy A). This is observed for each driving cycle. As less energy is circulating between the battery and SC, less energy is lost due to DC/DC conversion. Results show that the complexity added by predicting the DWT HFC does not reap benefits in terms of SC performance.

b) Difference between the real-time current demand and the DWT LFC (Strategy C) vs Difference between the real-time current demand and the predicted DWT LFC (Strategy D)

With strategy C, the SC takes over the current demand during the delay, consequently improving the SC assistance performance. A significant improvement of SC effective assistance during motoring, positive current rate, and braking is observed when comparing strategies C and D with strategies A and B for each driving cycle, as shown in Fig. 14. However, this improvement comes at the cost of higher energy circulation between the battery and SC, which increases energy losses due to DC/DC conversion.

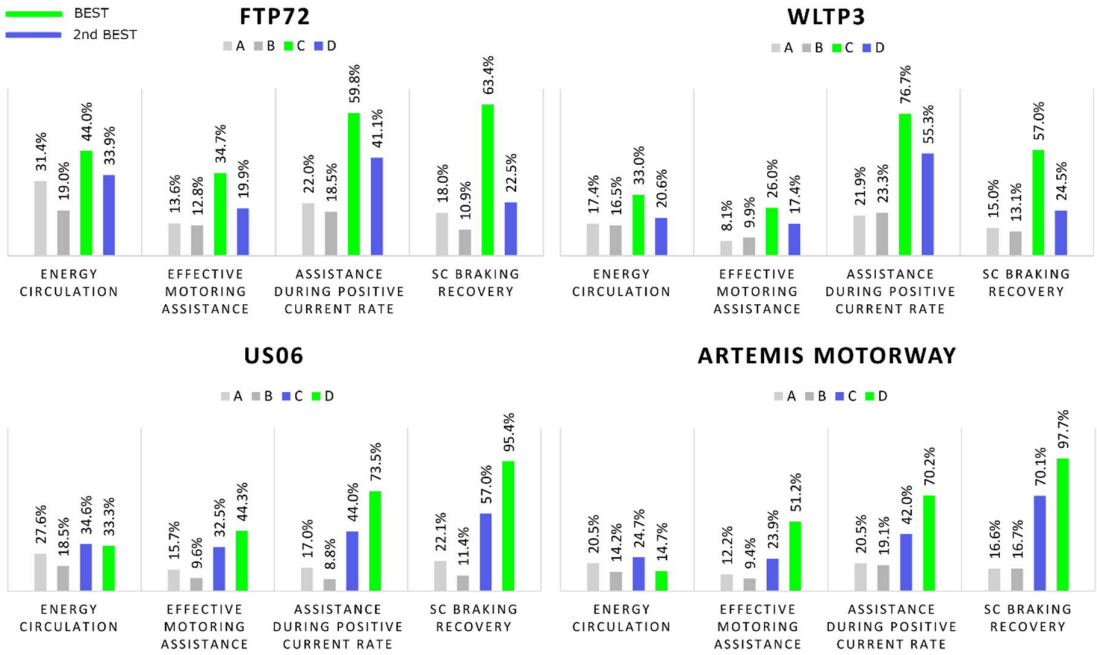

Fig 14. Results comparison

With strategy D, energy circulation and its associated energy losses are reduced as a consequence of delay compensation, when compared with strategy C. Meanwhile, SC performance does not improve for urban or mixed driving cycles (FTP72, WLTP3), but it does for highway driving cycles (US06 and Artemis Motorway). Strategy D provides good results over strategies A and B, however, its implementation in real time is complex. Furthermore, the variable prediction error obtained for different driving cycles as well the variable time required for the prediction algorithm excecution influences SC performance. Considering that the role of the SC is to assist the battery to cope with sudden power change and recover all regenerative braking, strategy C provides the best option as improves the SC performance in all driving conditions and it is easier to implement in real time. This, however, comes at a relatively higher cost of energy circulation which increases the system energy loss. Given the high efficiency of modern DC/DC converters, the advantages outweigh the disadvantages of this strategy.

V. CONCLUSIONS

In this paper, 4 different implementation strategies for a DWT based EMS, which produces frequency components with a delay of 4s with respect to the real time demand, have been evaluated using different metrics to quantify energy circulation and SC assistance during motoring, acceleration, and braking. The 4 strategies depend on how

the SC reference current is determined from the DWT with and without time delay compensation. For this purpose, a LSTM neural network to predict future power demand before it is fed to the DWT has been designed in order to compensate for the DWT time delay. Results show that obtaining the SC current reference as the difference between the real time current demand and the DWT LFC (strategy C) improves the SC assistance during motoring and braking when compared to the prediction based method in all driving conditions. Prediction proves to compensate for the delay and reduce energy circulation but it does not improve the SC performance. With aggressive driving cycles such as the US06 and Artemis motorway, the best results are obtained with a current reference calculated as the difference between the real time current demand and the predicted DWT LFC (strategy D). Real time implementation is, however, more difficult. Therefore, strategy C is chosen as the best control strategy to enable a DWT based EMS with 4s delay frequency components to perform in real time.

DWT filtration tools do not provide the same design flexibility and simplicity of implementation as conventional digital filters. A digital filter with an Infinite Impulse Response (IIR), for example, is usually implemented using analogue equivalents, which are used to find the continuous time filter transfer functions that approximate the frequency domain specifications using well established methods such as Butterworth, Chebyshev, Elliptic, and least squares. DWT, on the other hand, is limited by factors such as the choice of mother wavelet, where the Haar wavelet is the only option as it produces the smallest delay; and sampling rate, which influences the DWT decomposition and reconstruction dyadic tree's complexity.

Further work involves the development and experimental validation of an EMS based on a digital filter to obtain the SC current reference. The aim of the EMS will be to distribute energy efficiently by reducing energy circulation in the system, allocate all the generated braking energy to the SC and assist the battery during peak power demand. A comparison of the performance achieved with an EMS based on DWT and other based on digital filters will be carried to fill the gap in the literature regarding this topic and aid engineers in the selection of the most appropriate frequency sharing technique.

References

[1] The Faraday Institution, “High-energy battery technologies,” 2020.
[2] International Energy Agency, “Global EV Outlook 2019. Scaling-up the transition to electric mobility,” IEA Publications, 2019.
[3] M. Al Sakka, H. Gualous, N. Omar and V. Joeri, “Batteries and supercapacitors for electric vehicles,” in New Generation of Electric Vehicles, Intech, 2012.
[4] S. S. Williamson, Energy management strategies for electric and plug-in hybrid electric vehicles, Springer, 2013.
[5] Q. Zhang, W. Deng, S. Zhang and J. Wu, “A rule based energy management system of experimental battery/supercapacitor hybrid energy storage system for electric vehicles,” Journal of Control Science and Engineering, vol. 2016, 2016.
[6] W. Zhuo , R. Li, C. Zhuo, Y. Li, J. Xia and J. Liu, “Battery-supercapacitor hybrid devices: Recent progress and future prospects,” Advanced Science, vol. 4, no. 7, p. 1600539, 2017.
[7] A. Mansour, C. M. Hedi and B. Faouzi, “Experimental study of a pack of supercapacitors used in electric vehicles,” The Scientific World Journal, vol. 2017, 2017.
[8] M. Horn, J. MacLeod, M. Liu and J. Webb, “Supercapacitors: A new source of power for electric cars?,” Economic Analysis and Policy, vol. 61, pp. 93-103, 2019.
[9] Q. Xue, X. Zhang, T. Teng, J. Zhang, Z. Feng and Q. Lv, “A comprehensive review on classification, energy management strategy, and control algorithm for hybrid electric vehicles,” Energies, vol. 13, no. 20, p. 5355, 2020.
[10] T. Zimmermann, P. Keil, M. Hofmann, M. Horsche, S. Pichlmaier and A. Jossen, “Review of system topologies for hybrid electrical energy storage systems,” Journal of Energy Storage, vol. 8, pp. 78-90, 2016.
[11] M. Yan, M. Li, H. He, P. Jiankun and C. Sun, “Rule-based energy management for dual-source electric buses extracted by wavelet transform,” Journal of Cleaner Production, vol. 189, pp. 116-127, 2018.
[12] Q. Li, W. Chen, Z. Liu, M. Li and L. Ma, “Development of energy management system based on a power sharing strategy for a fuel cell-battery-supercapacitor hybrid tramway,” Journal of Power Sources, vol. 279, pp. 267-280, 2015.
[13] Y. Ates, O. Erdinc, M. Uzunoglu and B. Vural, “Energy management of an FC/UC hybrid vehicular power system using a combined neural network-wavelet transform based strategy,” International Journal of Hydrogen Energy, vol. 35, pp. 774-783, 2010.
[14] C. Zheng, H. Lian, T. Chen, Z. Cai and D. Fang, “A wavelet transform based power allocation strategy for lithium battery and ultracapacitor hybrid vehicular power systems,” in 31st Youth Academic Annual Conference of Chinese Association of Automation, Wuhan, 2016.
[15] J. Pan, J. Yan, Q. Tu and C. Jiang, “Fuzzy control and wavelet transform based energy management strategy design of a hybrid bulldozer,” Journal of Intelligent & Fuzzy Systems, vol. 29, pp. 2564-2574, 2015.
[16] X. Zhang, C. Mi, A. Masrur and D. Daniszewski, “Wavelet transform-based power management of hybrid vehicles with multiple on-board energy sources including fuel cell, battery and ultracapacitor,” Journal of Power Sources, vol. 185, pp. 1533-1543, 2008.
[17] O. Erdinc, B. Vural and M. Uzunoglu, “A wavelet-fuzzy logic based energy management strategy for a fuel cell/battery/ultra-capacitor hybrid vehicular power system,” Journal or Power Sources, vol. 194, pp. 369-380, 2009.
[18] S. Dusmez and A. Khaligh, “Wavelet-transform based energy and power decoupling strategy for a novel ultracapacitor-battery hybrid power split gear powertrain,” in IEEE Transportation Electrification Conference and Expo (ITEC), Detroit, 2013.
[19] S. Bourdim, T. Azib, K. Hemsas and C. Larouci, “Efficient energy management strategy for fuel cell ultracapacitor hybrid system,” in International Conference of Electrical Systems for Aircraft, Railway, Ship Propulsion and Road Vehicles & International Transportation Electrification Conference, Toulouse, 2017.
[20] Y. Zhang, S. Yang, S. Zhou and F. Chen, “Wavelet-transform algorithm application in hybrid power system optimization of electric vehicles,” Journal of Physics: Conference Series, vol. 1032, no. 4, 2019.

[21] C. Wang, R. Xiong, H. He, Y. Zhang and W. Shen, “Comparison of decomposition levels for wavelet transform based energy management in a plug-in hybrid electric vehicle,” Journal of Cleaner Production, vol. 210, pp. 1085-1097, 2019.
[22] Q. Zhang and W. Deng, “An adaptive energy management system for electric vehicles based on driving cycle identification and wavelet transform,” Energies, vol. 9, no. 5, p. 341, 2016.
[23] K. Lei and Z. Chen, “Energy management strategy based on adaptive wavelet analysis for HESS,” in IEEE 3rd International Electrical and Energy conference, Beijing, 2019.
[24] M. Masih-Tehrani, M. Ha'iri Yazdi, V. Esfahanian, M. Dahmardeh and H. Nehzati, “Wavelet based power management for hybrid energy storage system,” Journal of modern power systems and clean energy, vol. 7, pp. 779-790, 2019.
[25] M. Ibrahim, S. Jemei, G. Wimmer, N. Steiner, C. Kokonendji and D. Hissel, “Selection of mother wavelet and decomposition level for energy management in electric vehicles including a fuel cell,” International Journal of Hydrogen Energy, vol. 40, pp. 15823-15833, 2015.
[26] M. Robayo , M. Abusara, M. Mueller and S. Sharkh, “A smart energy management system for battery-supercapacitor in electric vehicles based on the discrete wavelet transform and deep learning,” in IEEE 29th International Symposium on Industrial Electronics, Delft, 2020.
[27] M. Ibrahim, J. Jemei, G. Wimmer and D. Hissel, “Nonlinear autoregressive neural network in an energy management strategy for battery/ultracapacitor hybrid electrical vehicles,” Electric Power Systems Research, vol. 136, pp. 262-269, 2016.
[28] Q. Zhang, L. Wang, G. Li and Y. Liu, “A real-time energy management control strategy for battery and supercapacitor hybrid energy storage systems of pure electric vehicles,” Journal of Energy Storage, vol. 31, 2020.
[29] E. Schaltz, “Electrical Vehicle Design and Modelling,” in Electric Vehicles - Modelling and Simulations, InTech, Available from: https://www.intechopen.com/books/electric-vehicles-modelling-and-simulations/electrical-vehicle-design-and-modeling, 2011.
[30] M. Ehsani, Y. Gao, S. Gay and A. Emadi, Modern Electric, Hybrid Electric, and Fuel cell vehicles, Boca Raton: CRC Press, 2004.
[31] O. Tremblay and L. Dessaint, “Experimental validation of a battery dynamic model for EV applications,” World Electric Vehicle Journal, vol. 3, no. 2, pp. 289-298, 2009.
[32] H. Miniguano, A. Barrado, C. Fernandez, P. Zumel and A. Lazaro, “A general parameter identification procedure used for comparative study of SCs models,” Energies, vol. 12, no. 9, p. 1776, 2019.
[33] R. Madan, S. Singh and N. Jain, “Signal filtering using discrete wavelet transform,” International Journal of Recent Trends in Engineering, vol. 2, no. 3, 2009.
[34] M. Schneiders, Wavelets in control engineering. Master's thesis, Eindhoven University of Technology, 2001.
[35] S. Siami-Namini, N. Tavakoli and A. Siami Namin, “A comparison of ARIMA and LSTM in forecasting time series,” in 17th IEEE International Conference on Machine Learning and Applications, Orlando, 2018.
[36] S. Venna, A. Tavanaei, R. Gottumukkala, V. Raghavan, A. Maida and S. Nichols, “A novel data driven model for real time influenza forecasting,” IEEE Access, vol. 7, pp. 7691-7701, 2018.
[37] X. Le, H. Ho, G. Lee and S. Jung, “Application of long short term memory (LSTM) neural network for flood forecasting,” Water, vol. 11, no. 7, p. 1387, 2019.
[38] J. Brownlee, Better Deep Learning. Train faster, reduce overfitting, and make better predictions, Machine Learning Mastery, 2020.
[39] J. Peng, R. Wang, L. Hongtao, Y. Zhou, H. Li, Y. Wu and Z. Huang, “A real-time layer-adaptive wavelet transform energy distribution strategy in a hybrid energy storage system of EVs,” Energies, vol. 12, no. 3, p. 440, 2019.
[40] J. Hu, D. Liu, C. Du, F. Yan and C. Lv, “Intelligent energy management strategy of hybrid energy storage system for electric vehicle based on driving pattern recognition,” Energy, vol. 198, 2020.
[41] Y. Shen, X. Yang, J. Sun and P. Liu, “Symlet wavelet transform based power management of hybrid energy storage system,” in 4th IEEE Conference on Energy Internet and Energy Systems Integration, 2020.
[42] K. Song, H. Chen, P. Wen, T. Zhang, B. Zhang and T. Zhang, “A comprehensive evaluation framework to evaluate energy management strategies of fuel cell electric vehicles,” Electrochimica Acta, vol. 292, pp. 960-973, 2018.
[43] F.Cignini,A.Genovese, F. Ortenzi, A. Alessandrini, L. Berzi, L, Pugi and R. Barbieri, “ Experimental data comparison of an electric minibus equipped with different energy storage systems,” Batteries, 2020